


## Numerical Investigation of the Optimum Angle for Open Channel Junction

Waqed H. Hassan<sup>1, 2</sup> , Nidaa Ali Shabat<sup>2\*</sup>

<sup>1</sup> Civil Engineering Department, Faculty of Engineering, University of Warith Al-Anbiyaa, Kerbala, Iraq.

<sup>2</sup> Civil Engineering Department, Faculty of Engineering, University of Kerbala, Kerbala, Iraq.

Received 08 December 2022; Revised 22 March 2023; Accepted 06 April 2023; Published 01 May 2023

### Abstract

Numerous natural and artificial streams, including those for irrigation ditches, wastewater treatment facilities, and conveyance structures for fish movement, have open channel confluences. The flow dynamics at and around the junction are intricate; in particular, immediately downstream of the junction, the flow creates a zone of separation on the inner wall along with secondary recirculation patterns. The structure of this complicated flow depends on several factors, including the flow rates in both channels, the angle of confluence, the geometry of the channels, including the longitudinal slope and bed discordance, the roughness of the boundary, and the intensity of the turbulence. It also has a significant impact on bed erosion, bank scouring, etc. The objective of the current work is to calculate the velocity profile and the separation zone dimensions for four angles (30°, 45°, 60°, and 75°) through the simulation process, and the best angle using a three-dimensional model. This work gives a detailed application of the numerical solution (Finite Volume) via Flow 3D software. Results for two flow discharge ratios,  $q^*=0.250$  and  $q^*=0.750$  were shown; the numerical model and the experimental results agreed well. The findings are consistent with past research and demonstrate how the main channel flow pattern is affected by changes in the channel crossing angle, as well as how greater separation zones are produced in the main channel when the flow discharge ratio  $q^*$  (main channel flow divided by total flow) is smaller. Analysis revealed that the separation zone's smallest diameter will be at the 75° crossing angle.

**Keywords:** Open Channel; Flow Pattern; Stream Lines; Junction Angle.

### 1. Introduction

Open channel junctions, which frequently occur in both natural and artificial river systems, including those for irrigation ditches, wastewater treatment facilities, and conveyance structures for fish movement, have open channel confluences and exhibit complex flow behavior. A transverse flow is the flow that actually results from the meeting of two flows that have different or comparable features. An increase in hydraulic resistance to the flow due to the introduction of a lateral flow into the main channel results in turbulent mixing and energy losses [1, 2]. The water depths before the junction are raised as a result of the mutual obstruction effects of the main channel and branch channel flows. The emergence of a shear plane that is skewed to a lesser or greater extent, depending on the difference in flow velocities of the branch and main channel flows, is another characteristic of open-channel junction flows. An unstable separation zone forms at the downstream corner of the junction as a result of the branch flow's deflection of the main flow towards the opposing bank [3, 4].

As a result, the combined flow's capacity in the channel is reduced, speeding the downstream flow and resulting in bed scouring and bank erosion. The byproducts of erosion may be deposited immediately below the area where erosion

\* Corresponding author: [nidaa.a@s.uokerbala.edu.iq](mailto:nidaa.a@s.uokerbala.edu.iq)



<http://dx.doi.org/10.28991/CEJ-2023-09-05-07>



© 2023 by the authors. Licensee C.E.J, Tehran, Iran. This article is an open access article distributed under the terms and conditions of the Creative Commons Attribution (CC-BY) license (<http://creativecommons.org/licenses/by/4.0/>).



has taken place or they may be transported over long distances to be deposited in the channels farther downstream. The turbidity of the water is raised by fine particles that are suspended in the mainstream. The erosion and deposition processes that take place at these locations alter the channel morphology over time, and the deposition of fine silt at the channel bottoms may cause the channel bed levels to rise and decrease channel capacities. Numerous variables, including stream discharge, junction angle, channel geometry, longitudinal slope, bank and bed resistance to flow (geology, including varieties of sediment), and Froude number, affect flow in channel junctions. Sediment movement at intersections complicates the flow behavior further; therefore, effective management of local sedimentation processes, channel scouring, sidewall erosion, and flooding, as well as sustainable river management, depends on a good understanding of the connections between flow dynamics, sediment transport, and bed morphology. Different methods have been employed in the past to study the dynamics of confluence flow. Theoretical studies, numerical studies, and field studies. These investigations offered important knowledge on the water surface, flow deflection, flow separation, secondary recirculation, shear layers, and velocity vector fields.

The initial research on the flow at open channel junctions was conducted by Taylor [5]. The author proposed an equation to calculate the water depth upstream of the junction using analytical methods. In their study on the size of the separation zone, Best & Reid [6] experimented with the effects of various confluence angles and discharge ratios. In their studies, Gurram et al. [7] looked at the separation zone, flow parameters, and lateral wall pressure force. In experimental studies at 30°, 45°, and 60° confluences, Hus et al. [8] examined the area downstream of the main channel where contraction and detachment flow from the inner wall.

Through experimental research, Weber et al. [9] investigated the flow rate, free surface depth, and kinetic energy of the turbulent flow. Numerous numerical studies utilized the information that these researchers acquired as a thorough base of data to validate them [10–15]. The velocity changes in post-junctions have been analyzed using a variety of computational models [13–16]. Using the CFD model, Bonakdari & Zinatizadeh [17] investigated the zone of separation in various discharges. Focusing on the subject of open channel flow rate measurement typically includes velocimetry, which is available in several methods. Doppler flow meters are being utilized to continuously measure the flow rate in open channels. These flow meters are built using measurements of the flow's depth and speed. They determine the flow rate using the continuity equation and the formula  $Q=A(h)*U(\text{mean})$ , which is the product of average velocity and wet cross-section. By taking into account precise geometrical data and the flow depth, cross-section  $A(h)$  is determined. Average velocity calculation requires specific expertise. In Doppler's scanned region, the velocimeter is a conical volume with a finite limit, and it measures the flow in a confined space [18]. This volume is used to determine the mean velocity for sensors, which is distinct from the mean cross-sectional velocity [17–21].

Particularly in regions where the velocity distribution is not uniform, such as the post-junction area, the mean velocity in the cross section differs from the velocity measured by the flow meter. Three-dimensional, rapid changes occur together with velocity in the region. Because it is derived from a small volume, the velocity measured by the flow meter cannot accurately represent the mean flow velocity [17, 22]. By numerically examining the impact of flow behavior on various flowmeters, Hilgenstock & Ernst [23] showed that ultrasonic flow meters may be numerically calibrated in a variety of situations. A flow meter located in a sewer was calibrated by Bollert & Bares [24] and Bonakdari [19] using the computational fluid dynamics technique. By using CFD modeling, Bonakdari & Zinatizadeh [17] investigated how the placement and design of Doppler flow meters affected the ability to monitor flow rates in open channels. They demonstrated that a straight channel's average velocity could not be determined using the measured velocity from sensors. If there is no possibility of sedimentation in the channel, the sensor put at the bottom of the channel can generate an accurate measurement.

By using a 3D computational model, Mignot et al. [25] investigated the flow configurations in junctions. According to the distance from the junction, the scientists examined how the intersection affected the velocity distribution. They claimed that the flow meter positioned at the channel's bottom, close to the junction locations, could have a 60% relative inaccuracy. In 90 open channel junctions, Sharifipour et al. [26] examined the impact of width and discharge ratio on the flow pattern and flow meter measurement accuracy. Al-Mussawi [27] demonstrates that the outcomes of the numerical simulation models demonstrate that a larger discharge ratio will require a shorter downstream distance from the junction to resume uniform flow. As a result, as the discharge ratio rises, so does the contraction coefficient. Rooniyan [28] Junction angles of 30°, 45°, and 60° were used in order to examine and assess how the shape of the channel junction affects the flow pattern and the diameters of the flow separation zone at various ratios of flow discharge (upstream channel discharge to total discharge of the flow).

Pandey & Mohapatra [29] in their numerical analysis focus on how continuous suction and blowing perturbations affect the reduction of the flow separation zone at a right-angled open channel junction using software for computational fluid dynamics. The results of the simulations, which were time-averaged, demonstrate that the sinusoidal perturbation is successful in reducing the size of the flow separation zone and, subsequently, the energy loss and bed shear stress. Pandey & Mohapatra [30] used the three-dimensional (3D) transient Reynolds-averaged Navier-Stokes equations to examine the propagation of flood waves at a right-angled merging open channel junction. Pandey et al. [31] calculated



the equivalent of Manning's roughness in combining open channel junction flows. The findings demonstrate that bed roughness and discharge ratio both influence the equivalent Manning's roughness in a channel junction flow. Nikpour & Khosravinia [32] studied the effects of a 45° side slope on the main channel's hydraulic properties of flow were examined and contrasted them with those at a 90° side slope. In this regard, the velocity field was assessed using an ADV for side slop angles of 45° and 90°. Using the discharge ratio and the dimensionless coordinates of the measured sites in the three-dimensional space of the flow field, the horizontal component of the flow velocity in the junction zone was estimated.

The majority of prior research on open channel confluences was focused on natural river confluences, where it is more challenging to control the environment. Moreover, open channels with oblique angles do not have any field modeling. For the researcher, numerical modeling of junction fluxes yields crucial information. It offers a chance to see how different flow phenomena in experiments produce distinct flow conditions. As a result, current research focuses on using numerical modeling to investigate junction flow behavior.

It has been thought of as a one-phase flow (water). To confirm that the numerical results have an appropriate level of accuracy, verification based on the experimental data was done. Cross sections with angles of 30°, 45°, 60°, and 75° confluence were studied specifically for velocity changes and dimensions of the separation zone. This study's major objective is to determine the velocity profile, dimension of the separation zone with various confluence angles, and the ideal angle at channel junctions using a 3D numerical model.

## 2. Materials and Methods

### 2.1. Experimental Data

In this study, the weber data were utilized to validate the numerical model. As seen in Figure 1, Weber et al. (2001) conducted studies in a lab setting using a 90° combined flow flume, the section taken in the current study has the following dimensionless  $x^* = 3$  to  $x^* = -9$ ,  $y^* = 1$  to  $y^* = -2$ . Different flow conditions could be created at the experimental facility as shown in Table 1.

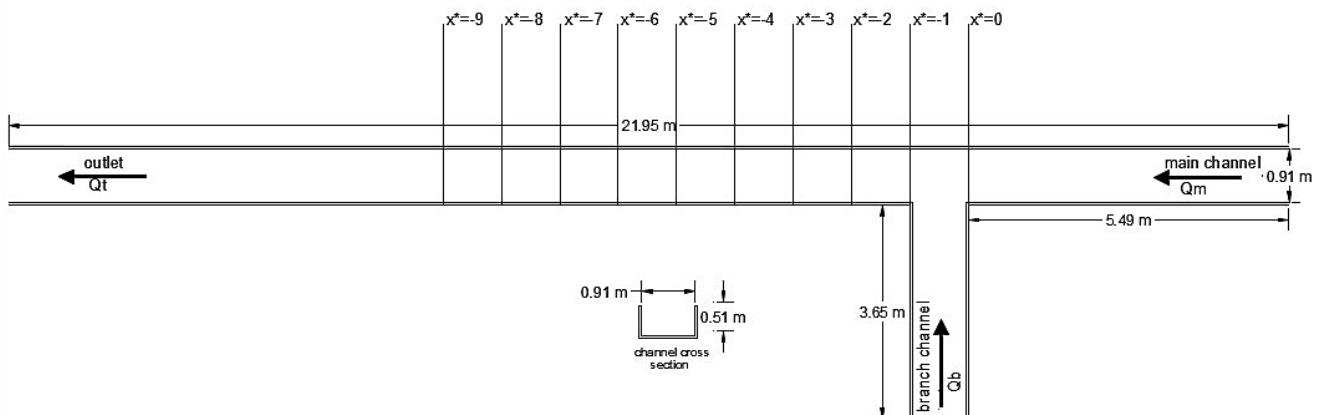


Figure 1. Experimental channel: Weber et al. (2001) [9]

Table 1. A list of experiments regulating hydraulic conditions

$Q_m$ (m <sup>3</sup> /s)	$Q_b$ (m <sup>3</sup> /s)	$Q^*$
0.042	0.127	0.250
0.099	0.071	0.583
0.127	0.042	0.750

Header tanks on both the main and branch channels provided varied discharge. The perforated plates and 100 mm thick honeycomb were put at the main and branch channel inlets to reduce the eddy that was formed at the inlets. The channel transition pieces were made smooth from vertical to horizontal, and the floor of the entire facility was kept horizontal to reduce losses on bends. The lengths of the main channel and branch channel are respectively 21.95 m and 3.66 m. 5.49 m downstream of the flume entrance is where the intersection is located. The downstream combined flow channel, main channel, and branch channel are all 0.914 m wide and 0.51 m deep. A constant downstream Froude number (0.37) and a constant tail-water average velocity (0.628 m/s) result from holding the total combined flow, 0.170 m<sup>3</sup> /s, and the tail-water depth, 0.296 m, constant. The values of the three-dimensional velocity indices have been rendered dimensionless by the usage of the downstream velocity.



The quantity  $q^*$  is obtained by dividing the upstream discharge from the main channel,  $Q_m$ , by the overall discharge,  $Q$ . The non-dimensionalized coordinates have the designations  $x^*$ ,  $y^*$ , and  $z^*$  for, respectively,  $x/w$ ,  $y/w$ , and  $z/w$ .

## 2.2. Assumptions

The problem was made simpler by making the following assumptions to model the junction flow indicated above. The flow was thought to be incompressible and stable, with average velocity components in the directions of  $u$ ,  $v$ , and  $w$ . As soon as the junction was reached, the water depth in the main and branch channels was deemed to be equal. This has been demonstrated by both experimental observations and prior analytical models. Side walls and the bed were seen as smooth walls, a sharp-edged, combined flow flume with horizontal slope was used in their testing setup.

## 2.3. Numerical Model Description

Over the past few centuries, numerical modeling has advanced quickly as processing power has increased to the point where it is now possible to solve problems numerically for a variety of applications. This advancement was causing numerical modeling to be used more frequently as a mainstream design method in many engineering domains. Despite the wide range of applications for numerical modeling, the fundamental ideas upon which all numerical models are built on analogous models, problems are set based on partial differential equations that represented the mathematical formalism of the specific instance. The formulation of a set of algebraic equations expressing the partial differential equations then makes use of several numerical technique types, such as finite element analysis or the technique of finite volume. The iterative or matrix solutions to these algebraic equations are then used to obtain an approximation of the solution. This method, though occasionally computationally taxing, enables the use of modern computing power, which is crucial for using numerical models. Most of the time, before being used in practice, the numerical model's alternatives are confirmed or set up by comparing them to observations or experiments involving physical models. Even after thorough model verification, sound engineering evaluation is still required to ensure the accuracy of any model output.

Flow 3D was an effective computing tool for mathematical modeling that could address a wide range of problems involving fluid flow. The aerospace industry, numerous casting types, inkjet printers, and many different hydroelectric generating stations have all benefited from new software applications. Flow 3D software divided the flow field into a rectangular-form-groove subdivision mesh into relatively small areas designated as cells, then calculated the numerical flow value to solve the Cartesian coordinates of the Navier-stock equations. Choosing an appropriate mesh on which to base the calculations is one of the most crucial steps in the flow modeling process. While numerical diffusion mistakes are more likely to occur with coarser meshes, they also take longer to solve. Therefore, it is necessary to strike a balance between the two. The answers might not be precise because of a variety of mistakes, including discretization and interpolation errors, depending on how the domain is discretized and the quality of the grid. Certain parameters must be managed to obtain reliable forecasts. To achieve the necessary accuracy, it's crucial to use the best cell dispersion possible. The size of the mesh cell could affect the simulation's timing accuracy; thus, it was crucial to lowering the size of the cell while maintaining acceptable flow details and sufficient resolution to capture key geometric elements. Starting with a somewhat big mesh and gradually reducing the mesh dimensions until the desired output did not vary appreciably with further mesh volume reductions has shown to be an effective method for determining the crucial mesh dimensions. A feature in Flow 3D that increased the amount of meshing in the various blocks. This enables the user to employ different meshes, including different mesh sizes and configurations, up until the point at which they restart the simulation using the data from the previous mathematical model's most recent time step.

For the purpose of developing various numerical approximations to the control equations, control volumes are built around each variable point. Surface fluxes, surface stresses, and body strengths for each control volume can be determined in relation to the values of the surrounding variables. Following that, these sums are combined to create an estimate for the protective regulations suggested by the movement equation. The general model was prepared and, in each example, an incompressible liquid and a free surface were used.

The fluid properties were set to those for water at 20°C for all simulations. Even though there are many more physical possibilities, just the two needed to be activated to deliver accurate simulations of the data needed for this inquiry. When gravity's vertical or  $z$ -direction acceleration reached  $-9.81\text{m/s}^2$ , the gravity option became activated. The option of viscosity and turbulence was also active when Newtonian viscosity and a suitable turbulence model were applied to the flow. As long as the two-equation  $k$ - $\epsilon$  model is selected, one turbulence model is employed and one of the Flow 3D models has been completely constructed. The block diagram of the numerical work is shown in Figure 2.



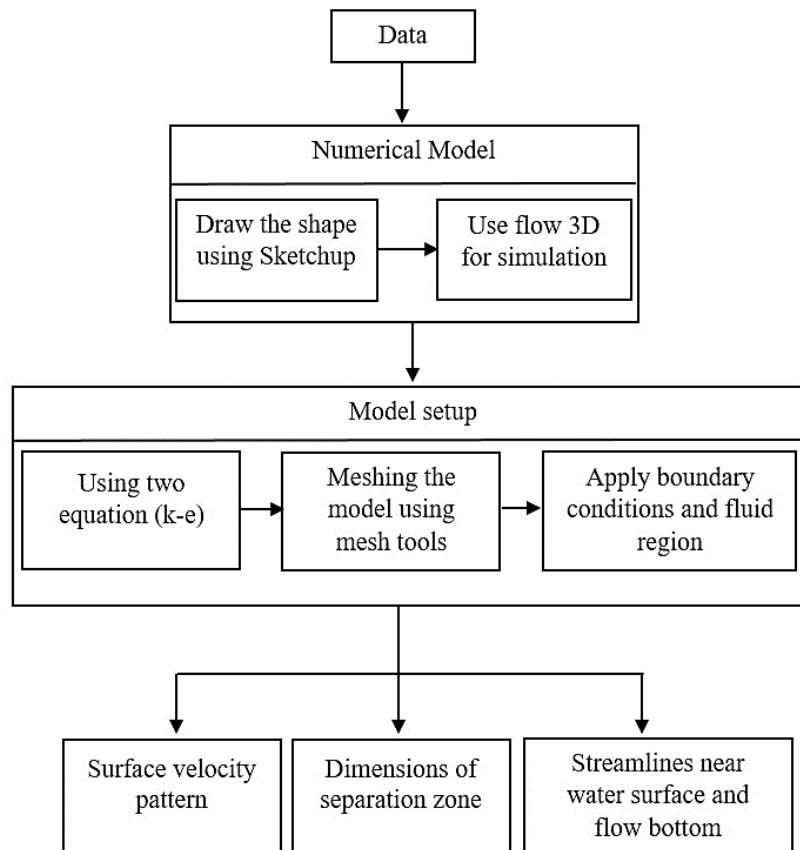


Figure 2. Block diagram of the proposed method

## 2.4. Governing Equations

Based on fundamental tenets of physics, such as the conservation of mass and momentum, the models resolve the entire set of three-dimensional Navier-Stokes equations. These equations describe how the local pressures and velocities inside the flowing fluid body are related. The Navier-Stokes equations and the continuity equation can both be expressed in general conservation from equation 1, making it simple to use them in the numerical program. This assists in streamlining and organizing the logic of a particular computer program. The net source within the cell is the difference between the outflow from the cell and the inflow into the cell, according to the fundamental balance or conservation equation. The dependent variables, such as phase mass, are the amounts being balanced. According to the general conserved variable " $\phi$ " the equations indicating the conservation of mass, momentum, and turbulent quantities can be expressed in the following way (PHOENICS 3.5 Manual).

$$\partial \frac{\rho(\phi)}{\partial t} + \frac{\partial}{\partial x_k} \left[ \rho U \phi - \Gamma \frac{\partial \phi}{\partial x_k} \right] = S_\phi \quad (1)$$

Convection, diffusion, temporal variation, and source terms are each represented by one of four terms in the balancing equation. Here,  $u, v, w$ , the turbulence values  $k$  and, etc., as well as other velocity component names, can all be represented as  $\phi$ .  $\rho$  is Fluid density ( $\text{kg/m}^3$ )  $U$  - Fluid velocity ( $\text{m/s}$ ),  $\Gamma$  is Diffusive Exchange Coefficient for  $\phi$  ( $\text{kg/ms}$ ),  $S_\phi$  is Source/sink term for  $\phi$  ( $\text{kg/m}^2\text{-s}^2$ ),  $\Gamma \phi$  is  $\rho (v_t + v_l)$  ( $\text{kg/m-s}$ ); where  $v_t$  ( $\text{m}^2/\text{s}$ ) and  $v_l$  ( $\text{m}^2/\text{s}$ ) are the turbulent and laminar viscosities respectively. The differential balancing equations are discretized and solved numerically.

## 3. Validation

In two cases, numerical results have been evaluated  $q^*=0.250$ , and  $q^*=0.750$ , and comparing the numerical results with experimental data has allowed for analysis of the numerical model's effectiveness in replicating the flow. Figure 3 and Figure 4 display the velocity, which have been made dimensionless, in  $q^*=0.250$  and  $q^*=0.750$  respectively, and  $x^*=-1$ ,  $x^*=-2$  cross-section. Both numerical and experimental charts at the inner wall of the main channel downstream  $y^*=0$  at  $q^*=0.250$  and  $x^*=-1$  show the negative velocity. In the separation zone, negative velocity indicates backflow toward the upstream. In the computed and experimental results, the high flow velocity has been specified close to the outer wall  $y^*=1$  cross-section. As the cross-section is positioned farther from the confluence zone, the difference between the two values decreases. In comparison to the 0.250 discharge ratio, the results for the 0.750 discharge ratio were more in line with the experimental data. At  $x^*=-1$ , the simulation error dropped by 24%, and at  $x^*=-2$ , the error dropped by 30%.



In both experimental and numerical simulations, the velocity near the outside wall is lower in the high discharge ratio compared to the low discharge ratio. The alternate flow won't have the main flow because the majority of the flow enters the junction from the main channel at a high discharge ratio, according to our analysis of the experimental and numerical results. As a result, the main flow deviates from its course less than when the discharge ratio is low, there is less flow turbulence, and the flow stabilizes more quickly after the junction. From Figures 3 and 4 it is clear that the numerical model used can simulate the flow when compared to the findings of the experiment.

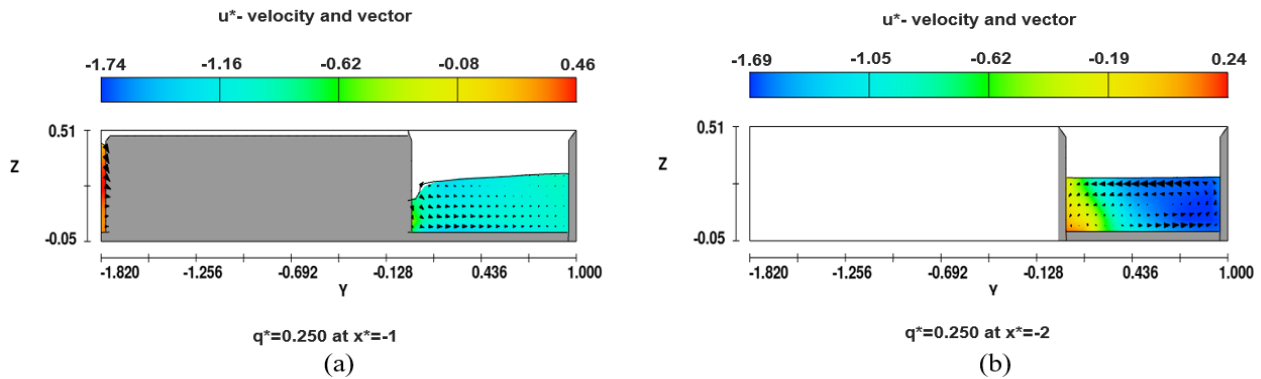


**Figure 3. Velocity Pattern in Cross-Sections of (a)  $u^*$ -Velocity contours at Cross Section  $x^*=-1$  for  $q^*=0.250$ ; (b)  $u^*$ -Velocity contours at Cross Section  $x^*=-2$  for  $q^*=0.250$**

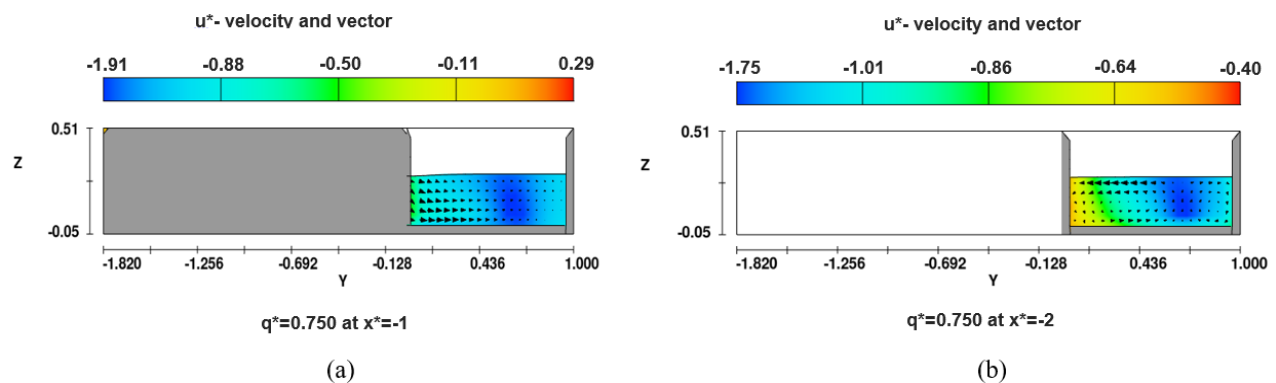


**Figure 4. Velocity Pattern in Cross-Sections of (a)  $u^*$ -Velocity contours at Cross Section  $x^*=-1$  for  $q^*=0.750$ ; (b)  $u^*$ -Velocity contours at Cross Section  $x^*=-2$  for  $q^*=0.750$**

## 4. Results and Discussion

The flow velocity lines at the  $x$ - $y$  plate for the four junctions (i.e.,  $30^\circ$ ,  $45^\circ$ ,  $60^\circ$ , and  $75^\circ$ ), for flow at the level  $Z^* = 0.278$ , and for flow close to the bed  $Z^* = 0.014$ , are shown in Figures 5 to 8. These diagrams were produced at the highest discharge ratio of flow  $q^*=0.750$  and the lowest discharge ratio of flow  $q^*=0.250$ , according to Table 1. It was found that the main and tributary channel flow combined to generate a secondary flow that was influenced by the junction angle and the flow discharge ratio. This secondary flow is turbulent and entirely three-dimensional. The main channel must be able to accommodate the additional flow as it enters the main channel while still preserving the overall mass balance. As a result, after the junction, the longitudinal flow velocities in the main channel increase. Velocity lines for various junction angles come closer to the right bank at the level and the left bank close to the bed. The free surface behaves like a wall with slip while the channel bed and side walls act as no-slip walls simultaneously. The overall outcome is a twist in the shear plane between the two interacting streams, which causes the separation zone from the bed to the free surface to have different sizes as shown in Table 2. This problem is a rise in the flow momentum differential between the level and the bed, which makes the level's flow separation zone dimensions bigger than those at the bed. The extent of the separation zone is less or disappeared near the channel bed in both the down streams and cross-stream directions than at the free surface for both flow conditions of  $q^*=0.250$ ,  $q^*=0.750$ . Additionally, it is evident that streamwise velocities rise after the junction in both  $q^*=0.250$  and  $q^*=0.750$  flow conditions. According to expectations, the separation zone extent decreases with increasing  $q^*$  because the main channel flow contributes more, when the water passes via a small-angle junction, the flow velocity is increased as shown in Figure 9 and Figure 10.



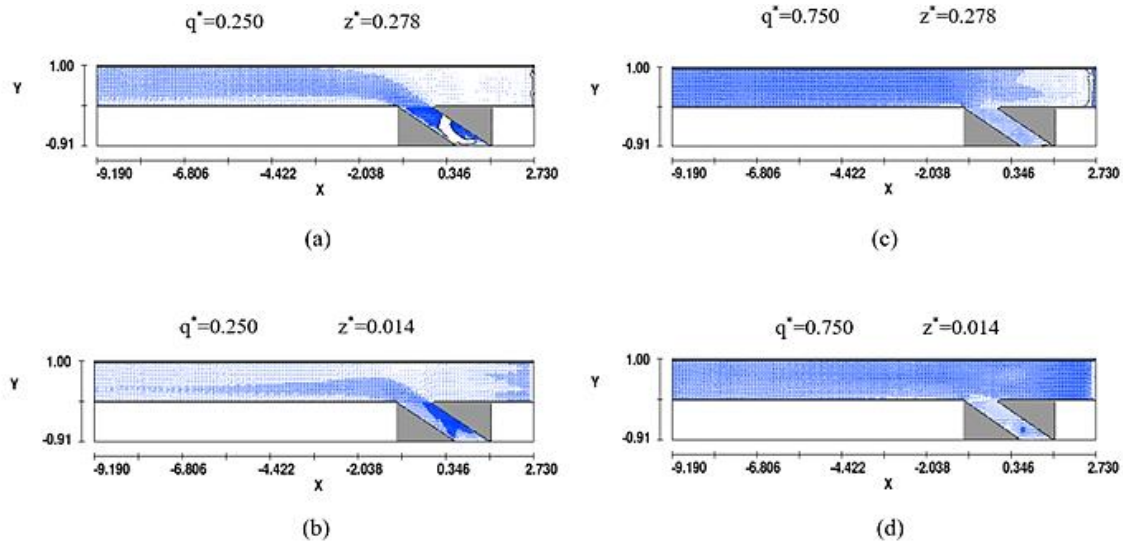


Figure 5. Stream lines at 30° junctions for (a)  $q^* = 0.250$  close to the surface of water; (b)  $q^* = 0.250$  a flow bottom; (c)  $q^* = 0.750$  close to the surface of water; (d) a flow bottom

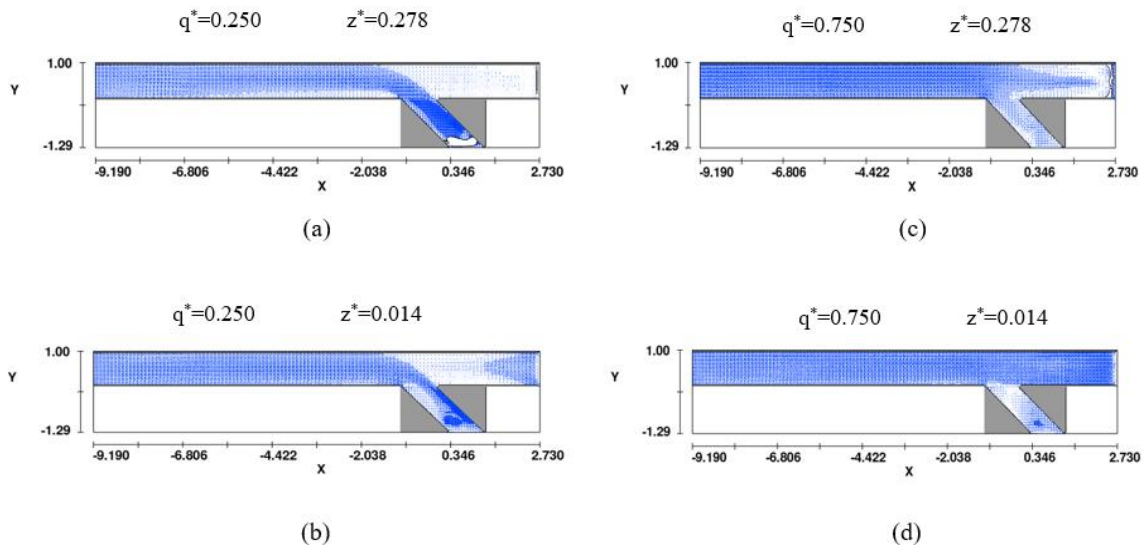


Figure 6. Streamlines at 45° junctions for (a)  $q^* = 0.250$  close to the surface of water; (b)  $q^* = 0.250$  a flow bottom; (c)  $q^* = 0.750$  close to the surface of water; (d) a flow bottom

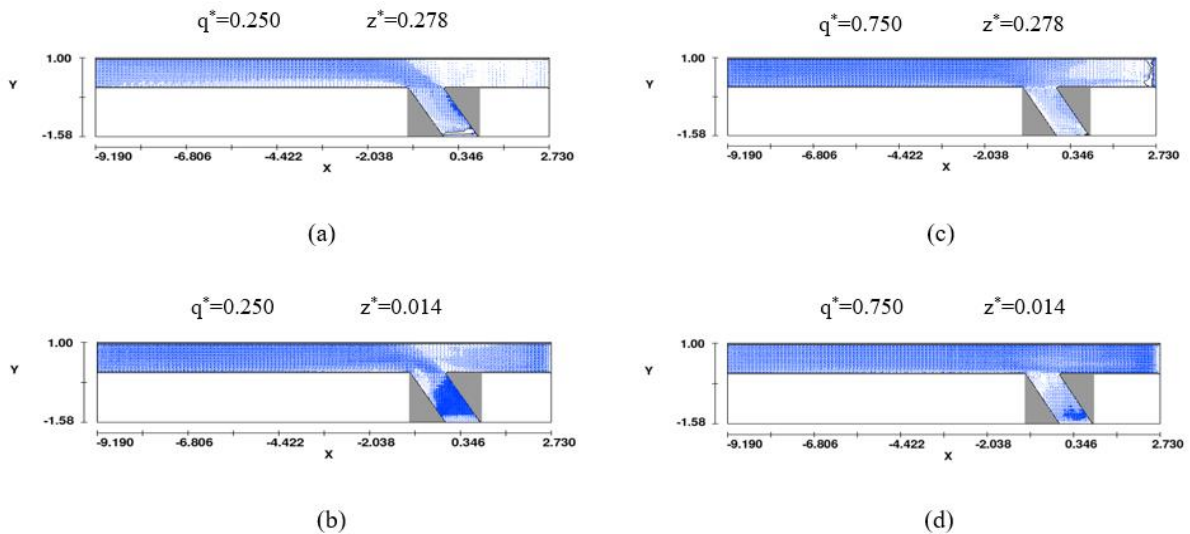


Figure 7. Streamlines at 60° junctions for (a)  $q^* = 0.250$  close to the surface of water; (b)  $q^* = 0.250$  a flow bottom; (c)  $q^* = 0.750$  close to the surface of water; (d) a flow bottom



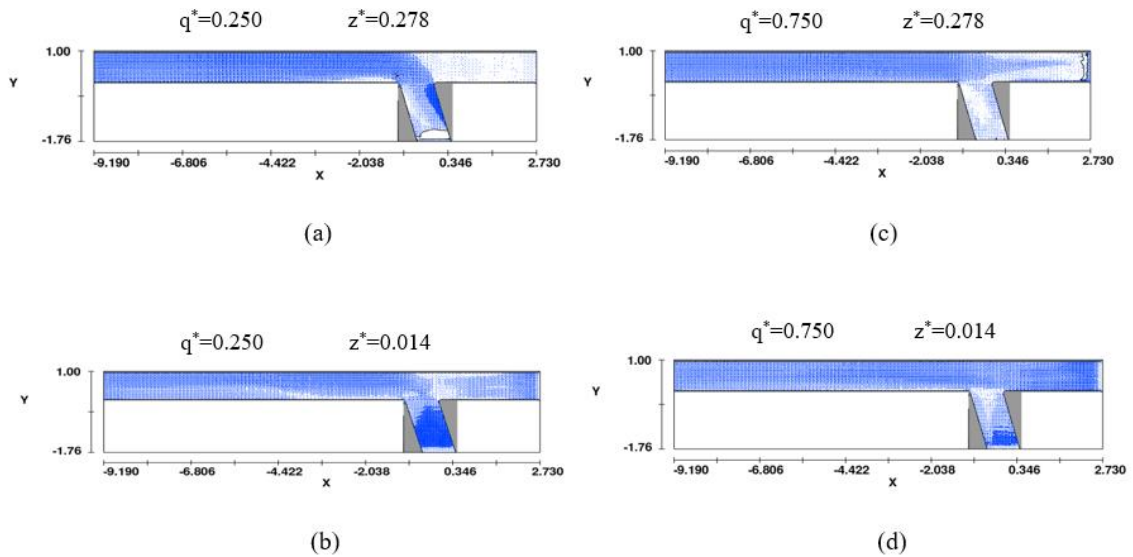


Figure 8. Stream lines at 75° junctions for (a)  $q^*=0.250$  close to the surface of water; (b)  $q^*=0.250$  a flow bottom; (c)  $q^*=0.750$  close to the surface of water; (d) a flow bottom

Table 2. Size of a separation zone

$\theta$	$q^*$	D	L	W
30	0.25	0.252	2.92	0.3
30	0.25	0.013	2.3	0.2
30	0.75	0.252	0.51	0.1
30	0.75	0.013	0	0
45	0.25	0.252	2.22	0.3
45	0.25	0.013	0	0
45	0.75	0.252	0	0
45	0.75	0.013	0	0
60	0.25	0.252	2.14	0.4
60	0.25	0.013	0	0
60	0.75	0.252	0	0
60	0.75	0.013	0	0
75	0.25	0.252	1.62	0.2
75	0.25	0.013	0.45	0.1
75	0.75	0.252	0	0
75	0.75	0.013	0	0

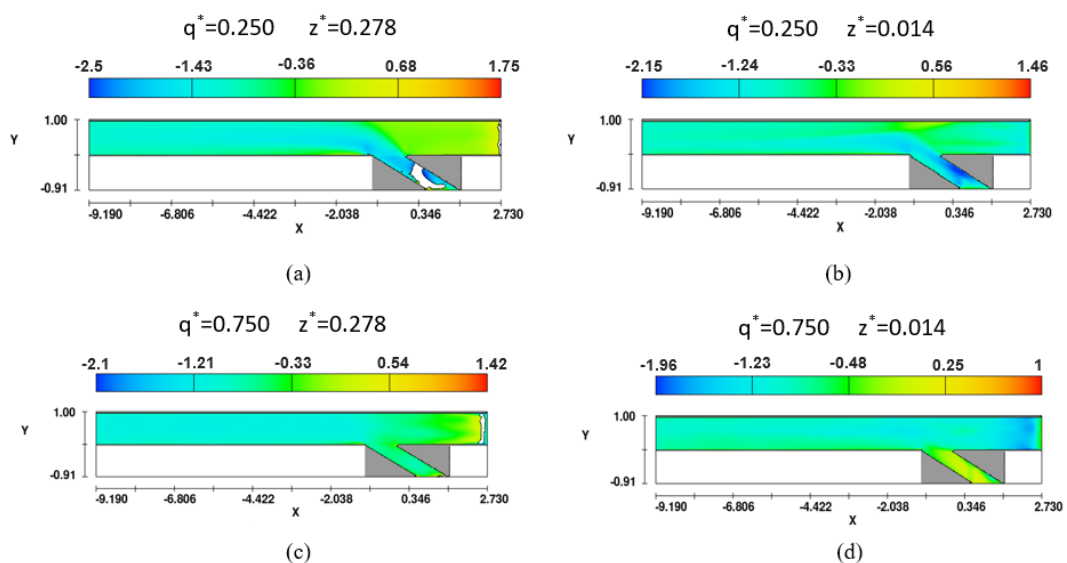
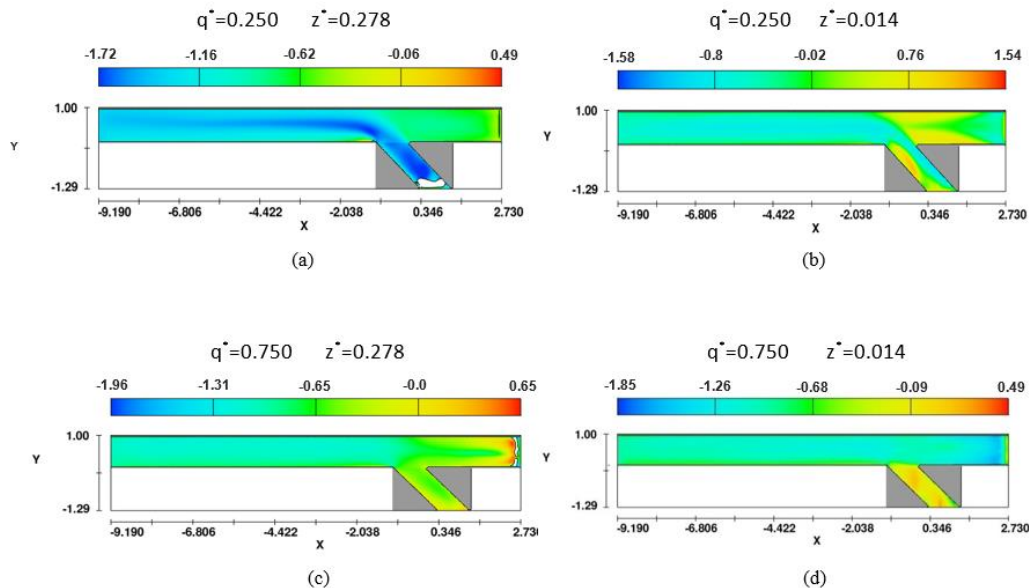


Figure 9. Surface velocity pattern at 30° junctions for (a)  $q^*=0.250$  near water surface; (b)  $q^*=0.250$  flow bottom; (c)  $q^*=0.750$  near water surface; (d)  $q^*=0.750$  flow bottom





**Figure 10. Surface velocity pattern at 45° junctions for (a)  $q^*=0.250$  near water surface; (b)  $q^*=0.250$  flow bottom; (c)  $q^*=0.750$  near water surface; (d)  $q^*=0.750$  flow bottom**

The  $u^*-v^*$  vector field in Figures 5 to 8 shows how the branch channel flow's entrance conditions alter noticeably between the surface and the bed. The surface flow is entering at a greater angle to the main channel, and the branch flow near the bed is significantly skewed downstream. As a result, the separation zone near the bed is smaller than the separation zone near the free surface. A recirculation zone is created when flow splits from the side wall at the junction's downstream corner. This could be explained by the fact that at lower discharge ratios, the flow from the branch channel is greater and the flow from the main channel is pushed more in the direction of the outer bank, resulting in a wider separation zone when  $q^*=0.250$ . Figure 3 shows the  $v^*-w^*$  vector field as flow advances downstream from  $x^*=-1$  to  $x^*=-2$ . Because there is more lateral momentum near the surface than towards the bed, the flow at  $x^*=-1$  shows surface water approaching the junction opposite the wall at  $y^*=1$ . The oncoming main channel flow somewhat deflects the surface water because there is a significant velocity component in the wall. Due to the weight of the water itself, it has been shown that the secondary recirculation pattern weakens as the flow moves downward and downstream.

## 5. Conclusion

This article investigates the flow profile and flow separation zone size at four junction angles of 30°, 45°, 60°, and 75° for flow ratios of  $q^*=0.250$  and  $q^*=0.750$  using Flow3D. This study was conducted because of the ongoing advancements in numerical modeling, the dearth of numerical studies on open channels with oblique angles, and the inability to control the dimensions, angles, discharge, etc. of the natural rivers that have been the subject of most prior studies. The results showed that the separating zone's size in the main channel will be smaller or non-existent when the main channel discharge is high and the discharge ratio is  $q^*=0.750$  because most of the produced turbulence will be drawn into the tributary channel. In addition, for a discharge ratio of  $q^*=0.250$  and at the junction angle, the high momentum of the tributary channel causes a turbulent zone to appear on the left side of the main channel. Additionally, the longitudinal velocity vectors are negative here. A separation zone's size increases from bed to level at a particular junction angle and constant flow ratio. The flow separation zone exists for all three discharge ratios, all junction angles, and at the 75° junction, where it reaches its minimum value for both flow ratios, making it the best angle for channel junctions, according to simulation data. For a particular junction angle, the size of the flow separation zone downstream of the main channel shrinks or disappears as the flow discharge ratio increases. Also, with a given discharge ratio and increased junction angle, separation zone dimensions shrink, a process that is apparent at level and close to the bed. Using channels of various lengths, angles, and discharges, as well as field models of inclined angles, it will be feasible to undertake a fresh study on open channels in the future. It will also be possible to simulate the results using another digital program.

## 6. Declarations

### 6.1. Author Contributions

Conceptualization, W.H.; methodology, N.A.S. and W.H.; software, N.A.S.; validation, N.A.S.; formal analysis, W.H. and N.A.S.; investigation, N.A.S.; resources, W.H.; data curation, N.A.S.; writing—original draft preparation, N.A.S.; writing—review and editing, W.H.; visualization, W.H.; supervision, W.H.; project administration, W.H. and N.A.S.; funding acquisition N.A.S. All authors have read and agreed to the published version of the manuscript.



## 6.2. Data Availability Statement

The data presented in this study are available on request from the corresponding author.

## 6.3. Funding

The authors received no financial support for the research, authorship, and/or publication of this article.

## 6.4. Conflicts of Interest

The authors declare no conflict of interest.

## 7. References

- [1] Hassan, W. H., & Jalal, H. K. (2021). Prediction of the depth of local scouring at a bridge pier using a gene expression programming method. *SN Applied Sciences*, 3(2), 159. doi:10.1007/s42452-020-04124-9.
- [2] Hassan, W. H., Hussein, H. H., Alshammari, M. H., Jalal, H. K., & Rasheed, S. E. (2022). Evaluation of gene expression programming and artificial neural networks in PyTorch for the prediction of local scour depth around a bridge pier. *Results in Engineering*, 13, 100353. doi:10.1016/j.rineng.2022.100353.
- [3] Al-Mussawi, W. H., Al-Shammari, M. H., & Alwan, H. H. (2009). Three-dimensional numerical investigation of flow at 90 ° open channel junction. *Journal of Kerbala University*, 7(4), 260–272.
- [4] Jalal, H. K., & Hassan, W. H. (2020). Three-dimensional numerical simulation of local scour around circular bridge pier using Flow-3D software. *IOP Conference Series: Materials Science and Engineering*, 745(1), 12150. doi:10.1088/1757-899X/745/1/012150.
- [5] Taylor, E. H. (1944). Flow Characteristics at Rectangular Open-Channel Junctions. *Transactions of the American Society of Civil Engineers*, 109(1), 893–902. doi:10.1061/taceat.0005772.
- [6] Best, J. L., & Reid, I. (1984). Separation Zone at Open-Channel Junctions. *Journal of Hydraulic Engineering*, 110(11), 1588 – 1594. doi:10.1061/(asce)0733-9429(1984)110:11(1588).
- [7] Gurram, S. K., Karki, K. S., & Hager, W. H. (1997). Subcritical Junction Flow. *Journal of Hydraulic Engineering*, 123(5), 447–455. doi:10.1061/(asce)0733-9429(1997)123:5(447).
- [8] Hsu, C.-C., Lee, W.-J., & Chang, C.-H. (1998). Subcritical Open-Channel Junction Flow. *Journal of Hydraulic Engineering*, 124(8), 847–855. doi:10.1061/(asce)0733-9429(1998)124:8(847).
- [9] Weber, L. J., Schumate, E. D., & Mawer, N. (2001). Experiments on Flow at a 90° Open-Channel Junction. *Journal of Hydraulic Engineering*, 127(5), 340–350. doi:10.1061/(asce)0733-9429(2001)127:5(340).
- [10] Huang, J., Weber, L. J., & Lai, Y. G. (2002). Three-Dimensional Numerical Study of Flows in Open-Channel Junctions. *Journal of Hydraulic Engineering*, 128(3), 268–280. doi:10.1061/(asce)0733-9429(2002)128:3(268).
- [11] Baghlani, A., & Talebbeydokhti, N. (2013). Hydrodynamics of right-angled channel confluences by a 2D numerical model. *Iranian Journal of Science and Technology - Transactions of Civil Engineering*, 37(C2), 271–283.
- [12] Ramamurthy, A. S., Qu, J., & Vo, D. (2007). Numerical and Experimental Study of Dividing Open-Channel Flows. *Journal of Hydraulic Engineering*, 133(10), 1135–1144. doi:10.1061/(asce)0733-9429(2007)133:10(1135).
- [13] Shakibainia, A., Tabatabai, M. R. M., & Zarrati, A. R. (2010). Three-dimensional numerical study of flow structure in channel confluences. *Canadian Journal of Civil Engineering*, 37(5), 772–781. doi:10.1139/L10-016.
- [14] Yang, Q. Y., Liu, T. H., Lu, W. Z., & Wang, X. K. (2013). Numerical simulation of confluence flow in open channel with dynamic meshes techniques. *Advances in Mechanical Engineering*, 2013, 860431. doi:10.1155/2013/860431.
- [15] Zaji, A. H., & Bonakdari, H. (2015). Application of artificial neural network and genetic programming models for estimating the longitudinal velocity field in open channel junctions. *Flow Measurement and Instrumentation*, 41, 81–89. doi:10.1016/j.flowmeasinst.2014.10.011.
- [16] Jalal, H. K., & Hassan, W. H. (2020). Effect of Bridge Pier Shape on Depth of Scour. *IOP Conference Series: Materials Science and Engineering*, 671(1), 12001. doi:10.1088/1757-899X/671/1/012001.
- [17] Bonakdari, H., & Zinatizadeh, A. A. (2011). Influence of position and type of Doppler flow meters on flow-rate measurement in sewers using computational fluid dynamic. *Flow Measurement and Instrumentation*, 22(3), 225–234. doi:10.1016/j.flowmeasinst.2011.03.001.
- [18] Sabbagh-Yazdi, S. R., & Bavandpour, M. (2022). Introducing ring collars and effective spiral threading elevation for cylindrical pier scour control. *Marine Georesources & Geotechnology*, 40(6), 639-654. doi:10.1080/1064119X.2021.1922555.



- [19] Bonakdari, H. (2006). Modeling of flows in sewers: application to the design of measurement points. Ph.D. Thesis, Université de Caen Normandie, Caen, France.
- [20] Koelling, C. (1996). SIMK-A new finite element model significantly improves the accuracy of flow measurements in sewers. 7<sup>th</sup> international conference on urban storm drainage, 9-13 September, 1996, Hannover, Germany.
- [21] Hassan, W. H., Hussein, H. H., & Nile, B. K. (2022). The effect of climate change on groundwater recharge in unconfined aquifers in the western desert of Iraq. *Groundwater for Sustainable Development*, 16, 100700. doi:10.1016/j.gsd.2021.100700.
- [22] Hughes, A. W., Longair, I. M., Ashley, R. M., & Kirby, K. (1996). Using an array of ultrasonic velocity transducers to improve the accuracy of large sewer mean velocity measurements. *Water Science and Technology*, 33(1), 1–12. doi:10.2166/wst.1996.0001.
- [23] Hilgenstock, A., & Ernst, R. (1996). Analysis of installation effects by means of computational fluid dynamics - CFD vs. experiments? *Flow Measurement and Instrumentation*, 7(3–4), 161–171. doi:10.1016/S0955-5986(97)88066-1.
- [24] Pollert, J., & Bares, V. (2002). Determination of velocity fields in a circular sewer. *International Conference on Sewer Operation and Maintenance*, Bradford, UK.
- [25] Mignot, E., Bonakdari, H., Knothe, P., Lipeme Kouyi, G., Bessette, A., Rivière, N., & Bertrand-Krajewski, J. L. (2012). Experiments and 3D simulations of flow structures in junctions and their influence on location of flowmeters. *Water Science and Technology*, 66(6), 1325–1332. doi:10.2166/wst.2012.319.
- [26] Sharifipour, M., Bonakdari, H., Zaji, A. H., & Shamshirband, S. (2015). Numerical investigation of flow field and flowmeter accuracy in open-channel junctions. *Engineering Applications of Computational Fluid Mechanics*, 9(1), 280–290. doi:10.1080/19942060.2015.1008963.
- [27] Al-Mussawi, W. H. (2009). Numerical analysis of velocity profile and separation zone in open channel junctions. *Al-Qadisiyah Journal for Engineering Sciences*, 2(2), 262-274.
- [28] Rooniyan, F. (2014). The Effect of Confluence Angle on the Flow Pattern at a Rectangular Open-Channel. *Engineering, Technology & Applied Science Research*, 4(1), 576–580. doi:10.48084/etasr.395.
- [29] Pandey, A. K., & Mohapatra, P. K. (2021). Reduction of the Flow Separation Zone at Combining Open-Channel Junction by Applying Alternate Suction and Blowing. *Journal of Irrigation and Drainage Engineering*, 147(10). doi:10.1061/(asce)ir.1943-4774.0001611.
- [30] Pandey, A. K., & Mohapatra, P. K. (2022). Three-Dimensional Numerical Simulation of the Flood-Wave Propagation at a Combining Open-Channel Junction. *Journal of Irrigation and Drainage Engineering*, 148(11). doi:10.1061/(asce)ir.1943-4774.0001713.
- [31] Pandey, A. K., Mohapatra, P. K., & Jain, V. (2020). Equivalent Manning's Roughness in Combining Open Channel Junction Flows. *World Environmental and Water Resources Congress 2020*. doi:10.1061/9780784482971.010.
- [32] Nikpour, M., & Khosravinia, P. (2021). Velocity Field Prediction in Open-Channels Junction using Data Driven Models. *Irrigation and Water Engineering*, 12(1), 104-121. doi:10.22125/iwe.2021.138256